Biomedicine & Pharmacotherapy 181 (2024) 117656

Contents lists available at ScienceDirect

Biomedicine & Pharmacotherapy

journal homepage: www.elsevier.com/locate/biopha

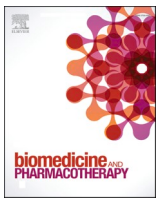

Chronic citalopram effects on the brain neurochemical profile and perfusion in a rat model of depression detected by the NMR techniques – spectroscopy and perfusion

Iveta Harastova-Pavlova [a,b], Eva Drazanova [a,c], Lucie Kratka [a], Petra Amchova [c], Maria Hrickova [c], Ondrej Macicek [a], Jiri Vitous [a,d], Radovan Jirik [a], Jana Ruda-Kucerova [c,*]

[a] Institute of Scientific Instruments of the Czech Academy of Sciences, Brno, Czech Republic
[b] Department of Condensed Matter Physics, Faculty of Science, Masaryk University, Brno, Czech Republic
[c] Department of Pharmacology, Faculty of Medicine, Masaryk University, Brno, Czech Republic
[d] Department of Biomedical Engineering, Faculty of Electrical Engineering and Communication, Brno University of Technology, Brno, Czech Republic

ARTICLE INFO

Keywords:
Citalopram
Depression
Brain metabolites
Olfactory bulbectomy
Cerebral perfusion
Rats

ABSTRACT

Background: Major depressive disorder (MDD) is a mental illness with a high worldwide prevalence and suboptimal pharmacological treatment, which necessitates the development of novel, more efficacious MDD medication. Nuclear magnetic resonance (NMR) can non-invasively provide insight into the neurochemical state of the brain using proton magnetic resonance spectroscopy (^{1}H MRS), and an assessment of regional cerebral blood flow (rCBF) by perfusion imaging. These methods may provide valuable *in vivo* markers of the pathological processes underlying MDD.

Methods: This study examined the effects of the chronic antidepressant medication, citalopram, in a well-validated MDD model induced by bilateral olfactory bulbectomy (OB) in rats. ^{1}H MRS was utilized to assess key metabolite ratios in the dorsal hippocampus and sensorimotor cortex bilaterally, and arterial spin labelling was employed to estimate rCBF in several additional brain regions.

Results: The ^{1}H MRS data results suggest lower hippocampal Cho/tCr and lower cortical NAA/tCr levels as a characteristic of the OB phenotype. Spectroscopy revealed lower hippocampal Tau/tCr in citalopram-treated rats, indicating a potentially deleterious effect of the drug. However, the significant OB model–citalopram treatment interaction was observed using ^{1}H MRS in hippocampal mI/tCr, Glx/tCr and Gln/tCr, indicating differential treatment effects in the OB and control groups. The perfusion data revealed higher rCBF in the whole brain, hippocampus and thalamus in the OB rats, while citalopram appeared to normalise it without affecting the control group.

Conclusion: Collectively, ^{1}H MRS and rCBF approaches demonstrated their capacity to capture an OB-induced phenotype and chronic antidepressant treatment effect in multiple brain regions.

1. Introduction

Major depressive disorder (MDD) is a mental illness with a significant global prevalence of around 19 % in adolescents [1] and 13 % in elderly populations [2]. This situation was exacerbated by the COVID-19 pandemic [3]. Depressed mood and anhedonia are the primary psychological symptoms, resulting in physical and social impairments [4–6] that can adversely affect the patient's quality of life, as well as impact their families and healthcare providers. The current standard pharmacological treatment for MDD exhibits a delayed onset, and pharmacoresistance is not uncommon, necessitating the development of novel, more efficacious MDD medications. The neurochemical state of the brain and cerebral perfusion are valuable parameters of the pathological processes underlying mental disorders, such as MDD [7,8], and both can be assessed using nuclear magnetic resonance (NMR) techniques. Furthermore, as the MDD rodent models have proved their validity [9,10], they may be beneficial in identifying non-invasive MDD biomarkers using the NMR method.

Proton magnetic resonance spectroscopy (^{1}H MRS) has been previously used to examine the neurochemical profile in MDD rodent models.

* Correspondence to: Masaryk University, Faculty of Medicine, Department of Pharmacology, Kamenice 5, Brno 625 00, Czech Republic.
E-mail address: jkucer@med.muni.cz (J. Ruda-Kucerova).

https://doi.org/10.1016/j.biopha.2024.117656
Received 4 July 2024; Received in revised form 22 October 2024; Accepted 28 October 2024
Available online 1 November 2024

Despite the various bias-introducing factors in these studies, several consistent outcomes have been observed [11]: in the hippocampus, a higher *myo*-inositol or *myo*-inositol to total creatine ratio, lower choline to total creatine, lower choline to *N*-acetyl aspartate, and higher taurine to total creatine were found, and in the cortex, higher choline to total creatine, higher glutamate, and a lower combination of glutamate and glutamine (Glx) or Glx to total creatine ratio were present. These results indicate affected local metabolism, neuronal dysregulation, inflammation, and a compensatory effect reaction [11], which is largely consistent with the pathophysiology observed in patients with MDD [12–14]. Although the acute and chronic effects of antidepressant treatment in the MDD rodent models have rarely been examined by ^{1}H MRS, partial normalisation of altered metabolite levels has been indicated [11].

Regional brain perfusion, commonly referred to as regional cerebral blood flow (rCBF), is a key parameter of the functional state of the brain, and depression in clinical trial participants has been associated with hypoperfusion [15,16] as well as increased regional blood perfusion [17] in numerous brain regions. Consequently, it is plausible that depression subtypes, such as MDD or bipolar disorder, possess their own unique perfusion signatures [18,19] with the potential to predict treatment response [20,21]. However, the utilization of rCBF in MDD animal models is infrequent, precluding the determination of the extent to which the animal models mimic the clinical situation.

The most effective utilization of the animal models involves their variable repeated use, and in this experiment, we used multiparametric NMR examination of the rat olfactory bulbectomy (OB) depression phenotype, which ^{1}H MRS has not yet examined.

Our pilot study focused on the brain's regional perfusion and metabolite profile as well as their lateralization tendencies given that the significant OB effect may be lateralized [22]. We observed no rCBF differences between the olfactory-bulbectomized rats and the controls [22], which is consistent with the only previous study in the same MDD model [23] and one recent forced-swim test model [24]. The single-voxel ^{1}H MRS revealed lower choline to *N*-acetyl aspartate, and lower choline to total creatine levels in the right dorsolateral hippocampus [22], while no differences were observed in the left dorsal hippocampus, and the right and the left sensorimotor cortex. Choline is a precursor of the neurotransmitter acetylcholine, which plays a crucial role in memory storage [25], and memory impairment is consistently reported in MDD patients [26], the OB model [27] and other animal MDD models [28]. Although this result appears justified, particularly in the memory-responsible brain structure, the hippocampus, it is unclear whether pharmacological treatment can reverse this phenomenon.

Therefore, in this study, we aimed to examine the effect of chronic antidepressant treatment, specifically citalopram (CIT), a widely utilized selective serotonin reuptake inhibitor, on the cerebral neurochemical profile and rCBF. Additionally, we considered the potential lateralization of the examined metabolites, an aspect that has been insufficiently explored in previous MDD model studies [11,22].

2. Methods

2.1. Animals

Fifty male adult albino Wistar rats weighing 350–450 g were obtained from the Central Animal Facility of Masaryk University, Brno, Czech Republic. The rats were single-housed in standard rodent polycarbonate cages with environmental enrichment (15 cm plastic tube 7.5 cm in diameter), and paper towels as nesting material. The rats were randomly divided into two groups: bulbectomised (OBX; n=30) and sham-operated (SHAM; n=20). A higher number of OBX rats was designated due to expected mortality during the surgery: eight rats were lost during the surgery (seven OBX and one SHAM). Subsequently, both SHAM and OBX rats were randomly divided into two groups treated with vehicle (VEH) or citalopram (CIT). Therefore, the final experimental groups were as follows: SHAM-VEH (n=10), SHAM-CIT (n=9), OBX-VEH (n=12), and OBX-CIT (n=11).

Environmental conditions were maintained constant throughout the study: relative humidity 50–60 %, room temperature 23 °C ± 1 °C, and normal 12-hour light-dark cycle (6 a.m. to 6 p.m. light). Food and water were provided *ad libitum* throughout the experiment. Following the surgery, pharmacological treatment, and behavioural testing, the rats were transferred to the Animal Facility at the Institute of Scientific Instruments of the Czech Academy of Sciences, Brno, Czech Republic, for NMR scanning and maintained under identical conditions as in the previous location.

All the procedures were performed in accordance with EU Directive No. 2010/63/EU and approved by the Animal Care Committee of the Faculty of Medicine, Masaryk University, Czech Republic, and Czech Governmental Animal Care Committee, in compliance with Czech Animal Protection Act No. 246/1992.

2.2. Drugs

Citalopram was utilized in the form of a commercially available preparation for human use (SEROPRAM® 40 mg/mL concentrate for infusion solution, Lundbeck A/S). The original solution was diluted with saline to a concentration of 10 mg/kg in 1 mL for intraperitoneal administration. Saline was employed as a vehicle at a dose of 1 mL/kg. Daily treatment was initiated 21–31 days after OB surgery and continued for 21 days. The treatment, subsequent behavioural tests and the NMR scanning were conducted sequentially due to the limited capacity of the NMR system (only 4 rats could be scanned daily owing to the duration of the experiment). Consequently, due to the higher number of OBX subjects, one rat from each experimental group was scanned daily when feasible. The outline of the study design is illustrated in Fig. 1.

2.3. Olfactory bulbectomy

Bilateral ablation of the olfactory bulbs under isoflurane anaesthesia was performed as previously described and repeatedly validated in the literature [22,29–34]. In brief, two burr holes, 2 mm in diameter, were drilled in the frontal bone 7 mm anterior from the bregma and 2 mm lateral from the bregma. Both olfactory bulbs were removed by aspiration. Prevention of blood loss from the ablation cavity was achieved by filling the dead space with a haemostatic sponge. The SHAM rats underwent identical anaesthetic and drilling procedures but with intact bulbs. A three-week period was allotted for recovery from the surgery and the development of the characteristic phenotype. During this period, the animals were handled for a few minutes daily to prevent any occurrence of aggressive behaviour [27,35]. At the conclusion of the experiments, the rats were euthanised by an anaesthetic overdose and the brains were dissected to confirm the success of the OB surgery.

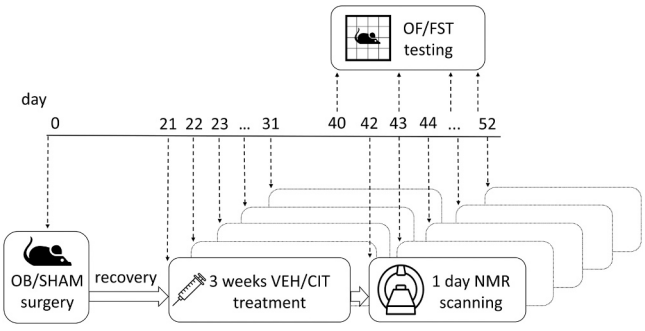

Fig. 1. : Timeline of the study. The graphic indicates the organisation of the study including the sequence of the procedures. Every working day 4 rats were scanned (one from each experimental group when possible) due to the technical limit to the number of NMR scans performed per day.

Further confirmation of the OB lesion was performed using anatomical MRI images. No rat was excluded due to brain damage or an inadequate lesion.

2.4. Behavioural testing

Behavioural testing was conducted during the last week of treatment, as illustrated in Fig. 1. This difference was necessitated by the requirement for sequential NMR scanning and to avoid weekend shifts. The forced-swim test was performed after the locomotor test on the same day.

2.4.1. Locomotor activity in a novel environment

An automated monitoring system (Actitrack® system, Panlab, Spain) was utilized to measure locomotor activity as described previously [36–39]. Each subject was individually placed in a reflective aluminium foil-wrapped monitoring cage for 10 min. Total locomotion was recorded and analysed in 1-min intervals. The number of faecal boli was documented after 10 min. The arena was subsequently cleaned with 1 % acetic acid to eliminate olfactory cues and dried prior to testing the next subject.

2.4.2. Forced-swim test

A modified forced-swim test [40] was employed to assess the immobility of the rats, as previously described [30,37]. The rats were placed into a 25 cm wide plexiglass cylinder filled with 30 cm of water (24 ± 1 °C). The sessions were video-recorded, and the water was replaced after each subject. A time-sampling scoring technique was employed, wherein the predominant behaviour, i.e. immobility, swimming or climbing, was recorded in each 5-second period of the 5-minute test. The test was conducted to evaluate spontaneous behaviour; therefore, there was no pre-test exposure to forced swimming, as is typically required for testing drug effects.

2.5. Nuclear magnetic resonance

All the animals were subjected to a single scan under anaesthesia with 2 % isoflurane and 1000 mL/min of oxygenated air on the day following the final treatment. The animals were maintained at a constant temperature through a water-heated bed holder, and their body temperature and respiration frequency were monitored throughout the entire measurement. This anaesthetic protocol was selected based on satisfactory prior experience in our laboratory and its compatibility to the NMR experiments. The total NMR-scanning duration ranged from 100 to 120 min per animal. A 9.4 T Bruker NMR small animal system (Bruker BioSpec 94/30 USR), volume transmitter coil (RF RES 400 1H 112/086 QSN) and 4-channel receiver array rat head coil (RF ARR 400 1H R.BR. LIN) were utilized to acquire the NMR data.

2.5.1. Proton magnetic resonance spectroscopy

The ^{1}H MRS single-voxel method was implemented in four brain regions: left and right dorsal hippocampus (LdHIPP, RdHIPP) and left and right sensorimotor cortex (LsmCTX, RsmCTX). These regions were selected based on biological and technical considerations, which are described in more detail in our pilot study [22], and to facilitate comparison with existing literature, and also with the pilot data [22]. Fig. 2 illustrates the location of the MRS-measured volumes (voxels) in the hippocampal and cortical regions, respectively, utilizing T1-weighted anatomical reference images. These images were acquired in all three orthogonal orientations (axial, sagittal, coronal) to ensure precise voxel (red polygons in Fig. 2) positioning and to mitigate partial volume artifacts from other brain structures. The reference images were scanned with the RARE pulse sequence: repetition time TR=1500 ms; echo time TE=5.8 ms; RARE factor 4; 1 average; field of view FOV=37.0 mm × 37.0 mm; image matrix 256 × 256; slice thickness 0.8 mm. In accordance with the Rat Brain Atlas [41], the centre of the LdHIPP and RdHIPP voxel was at −3.8 mm from the bregma, and the centre of the LsmCTX and RsmCTX was at 1.2 mm from the bregma. The voxel volumes were set to 7.8 mm^3 (1.5 mm × 1.3 mm × 4 mm) in the hippocampal regions and 12 mm^3 (3 mm × 1 mm × 4 mm) in the cortical regions. To obtain the single-voxel ^{1}H MRS signal the point-resolved spectroscopy (PRESS) pulse sequence was used: spectral width =4401.41 Hz; 4096 points; TR=2500 ms; TE=16.5 ms (TE1=8.85 ms, TE2=7.65 ms); 256 averages; 0.78 ms long 90°-Calculated excitation pulse; and two 1.05 ms long 180°-Calculated refocusing pulses. Outer volume suppression and water suppression (VAPOR) pulses were applied. First and second-order shimming was executed within the shimming volume (green polygons in Fig. 2) based on a previously measured B_0 map. Total acquisition time of the PRESS experiment was approximately 10 minutes and 40 seconds. The quality of the spectra was checked in the same way as in the pilot study, by the size of the line width of the water peak at 50 % height [42] and visually during the post-processing of the spectra.

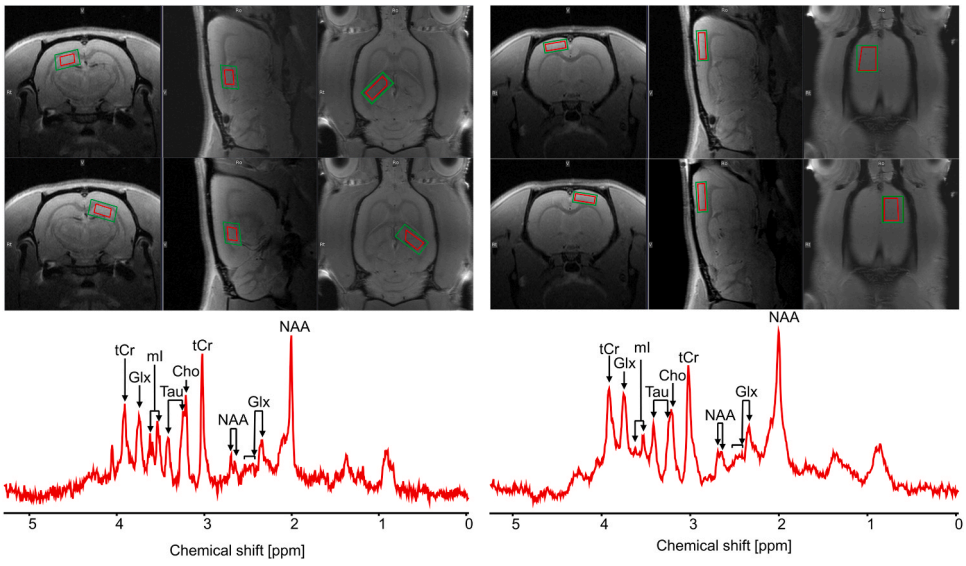

Fig. 2. : Voxel positioning in ^{1}H MRS experiments. Left part: position of the voxel in the hippocampi; below a representative hippocampal ^{1}H spectrum. Right part: position of the voxel in the cortices; below a representative cortical ^{1}H spectrum.

2.5.2. Regional cerebral blood flow

T1-weighted anatomical images were acquired before each arterial spin labelling (ASL) sequence using the RARE sequence with TR=1500 ms; TE=5.8 ms; RARE factor 4; 4 averages; FOV=37.0 mm × 37.0 mm; image matrix 256 × 256. Fifteen 1.25 mm-thick axial slices covered the brain from the root of the olfactory bulbs to the cerebellum. The anatomical image reference for the ASL sequence settings can be found on the left of Fig. 3. Due to biological and technical reasons [22], and the necessity to compare the results, as in our previous studies [22,43,44], one axial perfusion slice was positioned −3.8 mm from the bregma [41]. A 2D LL-FAIR with the golden-angle radial readout and its parameters was derived from Vitouš et al. [45] except for slice thickness ST=1.25 mm, TR=7 ms, FOV=37.0 mm × 37.0 mm and FA=5°. In total, 80000 spokes were acquired, resulting in an acquisition time (TA) of 9 minutes and 21 seconds.

2.6. Data processing

2.6.1. ^{1}H MRS data processing

The MRS data were processed using the free clinical and biomedical spectroscopic software package jMRUI [46]. A simulated metabolite basis set is needed to quantify the metabolites in the spectra. This was made in part of the jMRUI software, the NMR-ScopeB [47]. The basis set included creatine (Cr), phosphocreatine (PCr), *N*-acetyl aspartate (NAA), choline (Cho), glutamate (Glu), glutamine (Gln), *myo*-inositol (mI) and taurine (Tau), and was used in the model function in the new fully automated version of the QUEST [48] algorithm, QUEST-MM [49]. After metabolite quantitation, the relative concentrations for each ^{1}H MRS-examined brain region were expressed: Cho/NAA, Cho/tCr, NAA/tCr, Glx/tCr, mI/tCr, Tau/tCr, Glu/tCr, and Gln/tCr, where tCr=Cr+PCr and Glx=Glu+Gln. As well as the hemispheric metabolite ratios, the averaged values were also calculated. The representative spectra from the hippocampus and cortex are depicted at the bottom of Fig. 2. Four spectra from the LsmCTX were excluded from further analysis as significant remains were detected after a visual check of the fitted spectra residue. The accuracy of metabolite amplitude fitting is expressed as Cramer-Rao lower bounds: SD of metabolites' amplitudes in percents (depicted in Table 1).

2.6.2. ASL data processing

The ASL data were used to calculate the T1 relaxation maps in the selective and non-selective case, which were later used to compute the CBF values according to the equation in the research by Belle et al. [50]. The regions of interest (ROIs) in the perfusion maps were manually drawn by a blinded researcher using a script written in MATLAB (The MathWorks Inc., Natick, MA, USA) according to the Rat Brain Atlas [41] and statistically analysed. The examined ROIs depicted in the central part of Fig. 3 were: the whole brain, the circle of Willis (cWillis), the left and the right sensorimotor cortices (the average of both was used for analysis – smCTX), the left and the right piriform cortex (the average of both was used for analysis – pirCTX), the left and the right dorsal hippocampus (the average of both was used for analysis – dHIPP), the left and the right thalamus (the average of both was used for analysis – THAL).

Table 1
Cramer-Rao lower bounds of the estimated metabolites in ^{1}H MRS results.

Estimated metabolite	CIT AVG CRLB [%]	Estimated metabolite	CIT AVG CRLB [%]
Cho RdHIPP	6.57	Cho RsmCTX	6.89
Cr RdHIPP	13.23	Cr RsmCTX	38.51
Glu RdHIPP	6.31	Glu RsmCTX	5.83
Gln RdHIPP	15.54	Gln RsmCTX	16.43
mI RdHIPP	4.29	mI RsmCTX	6.96
NAA RdHIPP	3.24	NAA RsmCTX	2.58
PCr RdHIPP	24.09	PCr RsmCTX	15.66
Tau RdHIPP	5.65	Tau RsmCTX	4.09
tCr RdHIPP	11.13	tCr RsmCTX	12.84
Glx RdHIPP	4.84	Glx RsmCTX	4.42
Cho LdHIPP	6.72	Cho LsmCTX	5.63
Cr LdHIPP	16.29	Cr LsmCTX	42.15
Glu LdHIPP	6.4	Glu LsmCTX	4.89
Gln LdHIPP	14.29	Gln LsmCTX	13.08
mI LdHIPP	3.81	mI LsmCTX	5.16
NAA LdHIPP	3.33	NAA LsmCTX	2.25
PCr LdHIPP	16.52	PCr LsmCTX	13.92
Tau LdHIPP	4.9	Tau LsmCTX	3.81
tCr LdHIPP	10.21	tCr LsmCTX	11.6
Glx LdHIPP	4.83	Glx LsmCTX	3.71

The accuracy of metabolite amplitude fitting expressed using Cramer-Rao lower bounds; percentual SD of fitted metabolites' amplitudes.

2.7. Statistical analysis

All data were summarised as means±SEM. Statistical analysis was performed using Statistica 14.0.0.15 (TIBCO Software Inc.). Normality was tested using the Shapiro-Wilk normality test, and all data was parametric. The dataset features two main factors: the OB model and the CIT treatment. Therefore, 2-way ANOVA was used, followed by the Fisher LSD post-hoc test when the interaction of the factors was significant. In all statistical tests, the boundary of statistical significance was set to $p<0.05$.

3. Results

3.1. Behavioural profile

The locomotor activity test yielded the expected OB-induced phenotype. The 2-way ANOVA revealed initial hyperactivity in the OBX group in the first minute of the 10-minute test ($F(1,37)=7.16$, $p=0.011$). The number of faecal boli, as an indirect measure of emotionality, showed a significant effect of the OB model: $F(1,37)=15.39$, $p<0.001$, CIT treatment: $F(1,37)=7.95$, $p=0.008$ and interaction of the factors: $F(1,37)=4.27$, $p=0.046$. The Fisher LSD post-hoc test indicated that the OBX-VEH rats produced more faecal boli than the

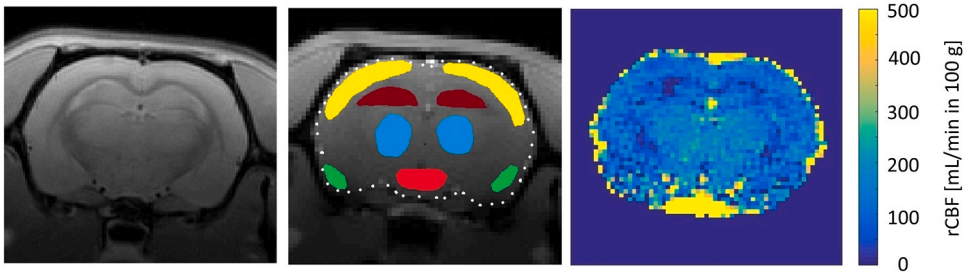

Fig. 3. : rCBF experiment. Left part: anatomical reference image. Central part: the delineation of regions of interest in a 2D-LL FAIR image (bregma -3.8 mm); colour codes: sensorimotor cortex - yellow, piriform cortex - green, hippocampus - brown, thalamus - blue, circle of Willis – red, whole brain – white dotted. Right part: perfusion map in one representative OBX animal; rCBF colour scale in mL/min in 100 g of brain tissue.

SHAM-VEH ($p<0.001$), SHAM-CIT ($p<0.001$), and OBX-CIT ($p<0.001$) rats. The forced-swim test did not indicate the effect of the OB model. However, it did show an effect of the CIT treatment in increased swimming behaviour. All behavioural results are depicted in Fig. 4 together with detailed statistical results from the analysis of the forced-swim test data.

3.2. ^1H MRS data

3.2.1. Dorsal hippocampus

The OB model effect (**A**, **B** in Fig. 5) and the CIT treatment effect (**C** in Fig. 5) were revealed in the hippocampal region: lower levels of Cho/tCr were shown in the OB model than in the SHAM rats in the LdHIPP: $F(1,38)=6.19$, $p=0.017$, and the averaged dorsal hippocampus (dHIPP): $F(1,38)=4.91$, $p=0.033$, while Tau/tCr levels were shown to be lower in the dHIPP of the CIT-treated rats than the control ones: $F(1,38)=4.51$, $p=0.040$.

The top parts of **D-I** in Fig. 5 show the interactions of the OB-CIT factors: a different effect of the CIT treatment on the SHAM and the OBX group. The bottom parts of **D-I** in Fig. 5 display the group differences revealed by the Fisher LSD post-hoc test. In the RdHIPP (**D** in Fig. 5), only mI/tCr showed any significant factors' interaction: $F(1,38)=6.63$, $p=0.014$ and the post-hoc test revealed lower values in the SHAM-CIT group compared to the SHAM-VEH rats ($p=0.031$). Furthermore, in the LdHIPP a significant interaction of the main factors was detected in Gln/tCr (**E** in Fig. 5): $F(1,38)=5.26$, $p=0.027$ and the post-hoc test revealed lower values in the SHAM-CIT group compared to the SHAM-VEH rats ($p=0.014$). Also, a significant interaction of the factors in Glx/tCr was found: $F(1,38)=4.84$, $p=0.034$ in the LdHIPP (**F** in Fig. 5). However, the post-hoc test did not identify a significant difference among the experimental groups. Averaged values from this brain region confirmed the findings from the hemispheres. The OB model-CIT treatment interaction was significant in mI/tCr: $F(1,38)=5.47$, $p=0.025$ and Gln/tCr: $F(1,38)=8.86$, $p=0.005$ in the dHIPP (**G, H** in Fig. 5), and the post-hoc test showed lower values of mI/tCr in the SHAM-CIT group compared to the SHAM-VEH rats ($p=0.019$). In relation to Gln/tCr, the SHAM-VEH rats showed a higher ratio than the SHAM-CIT ($p=0.012$) and the OBX-VEH ($p=0.023$) groups. A significant interaction of the factors was also shown in the averaged hippocampal Glx/tCr (**I** in Fig. 5): $F(1,38)=6.35$, $p=0.016$, however the post-hoc test rendered non-significant intergroup's results. All the ^1H MRS data from the hippocampus are summarised in Table 2, along with full statistical details.

3.2.2. Sensorimotor cortex

In the cortical region, only an OB model effect was revealed (Fig. 6): NAA/tCr was shown to be lower in the OB model than in the SHAM rats in the RsmCTX: $F(1,38)=5.98$, $p=0.019$ and the averaged sensorimotor cortex (smCTX): $F(1,34)=7.18$, $p=0.011$. No significant CIT treatment effect or any interaction of the main factors was found in the cortical regions. All the ^1H MRS data from the cortex are summarised in Table 3, along with full statistical details.

3.3. rCBF data

The two-way ANOVA did not reveal the main factors (the OB model and the CIT treatment) effect but did reveal their significant interaction in the cWillis (**A** in Fig. 7), the whole brain (**B** in Fig. 7), the dHIPP (**C** in Fig. 7) and the THAL (**D** in Fig. 7). The post-hoc test indicated a significantly higher perfusion in the OBX-VEH group compared to the SHAM-VEH in the whole brain ($p=0.031$), dHIPP ($p=0.004$) and THAL ($p=0.009$). The differences were normalised by the chronic CIT treatment in the OB model (whole brain: $p=0.006$, dHIPP: $p<0.001$, THAL: $p<0.001$) while having no effect in the control group. The rCBF results are depicted in Fig. 7, and full statistical details are in Table 4.

4. Discussion

This study reports novel data obtained utilizing two NMR techniques in an OB rat model of depression. The rats' behavioural profile confirmed the anticipated OB model effect: a higher novelty-induced

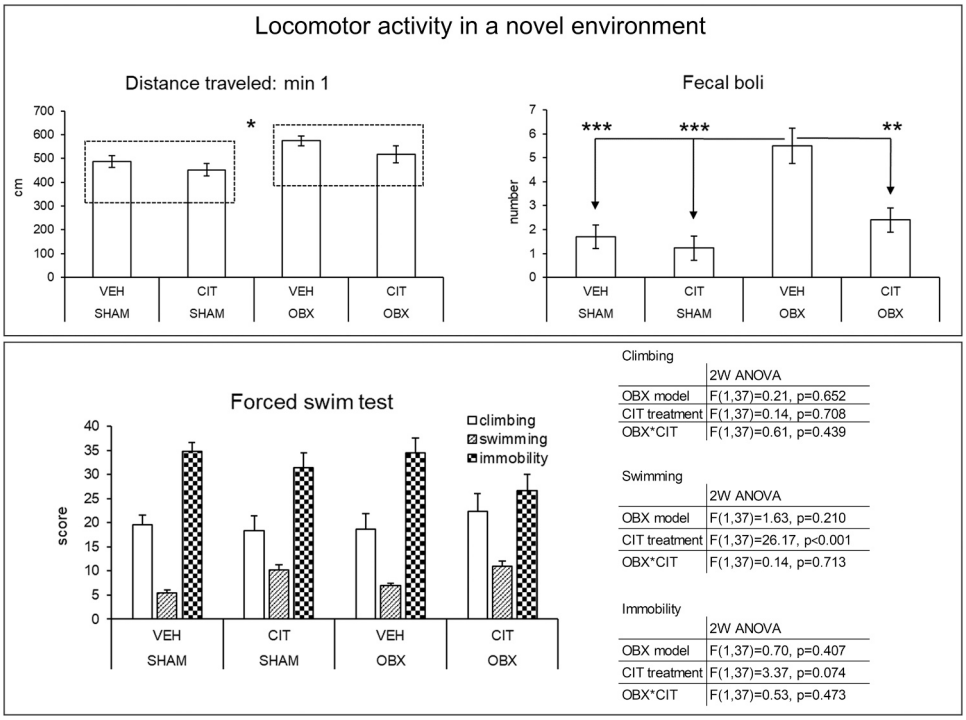

Fig. 4. : Behavioural results. The bar graphs show the mean ± SEM of the behavioural variables. The top graphs show the results of the locomotor test, i.e. distance travelled in the first minute and number of faecal boli over 10 minutes of the test. The bottom graph shows the behaviour in the forced-swim test and the table shows statistical results from this test. *$p<0.05$, **$p<0.01$, ***$p<0.001$.

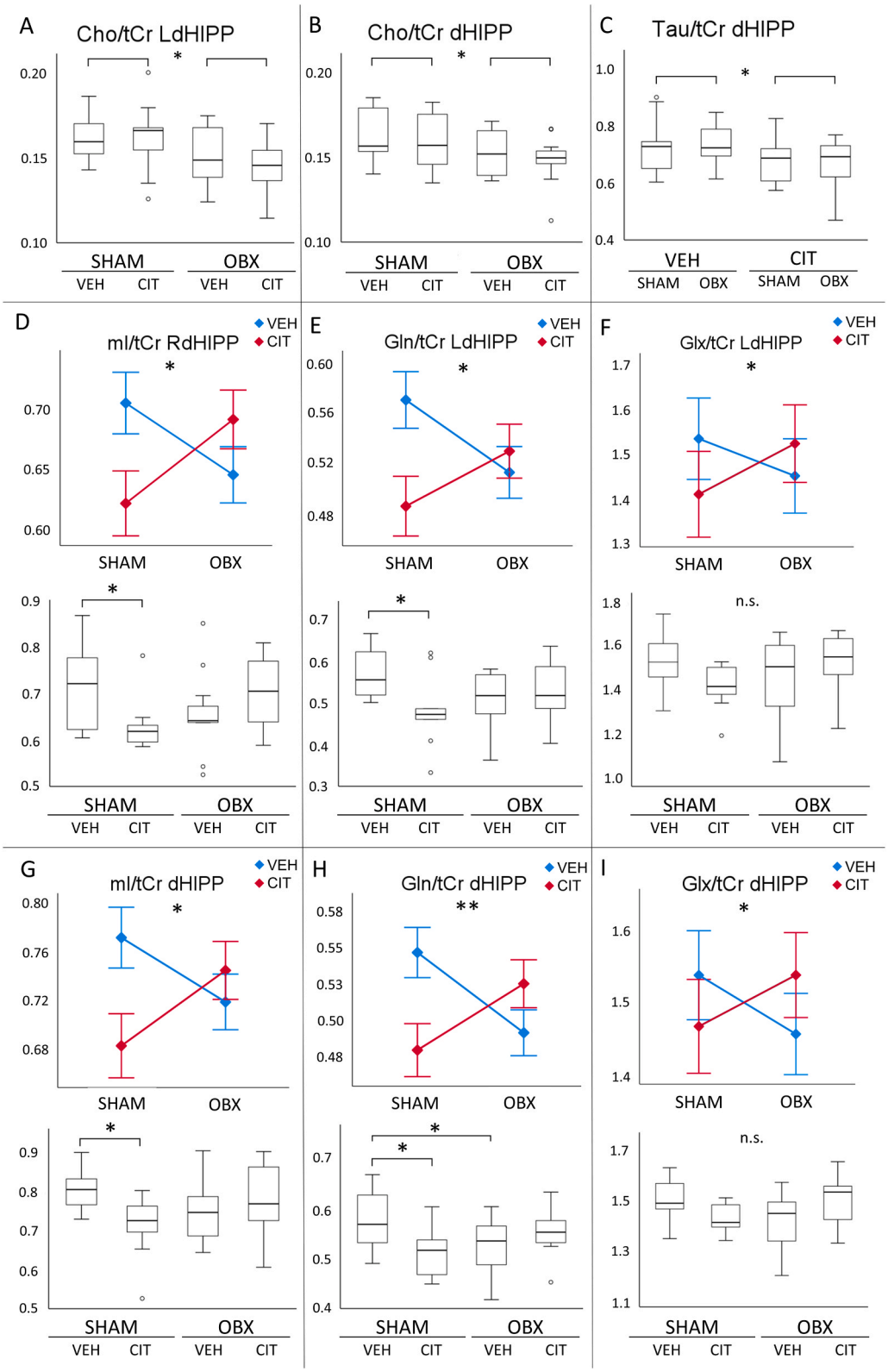

Fig. 5. : ^{1}H MRS results – dorsal hippocampus. A, B – olfactory bulbectomy model effect and C – citalopram treatment effect on relative metabolite concentrations. D-I – top parts show the interactions of the study's main effects: OB model-citalopram treatment on relative metabolite concentrations. D-I – bottom parts show the group differences revealed by the LSD post-hoc test. In the boxplots, whiskers display the maximum and minimum values (except outliers - ○), top of the box is quartile 3, line inside the box is median, and bottom of the box is quartile 1 (*p<0.05).

Table 2
^{1}H MRS data from the dorsal hippocampus.

	SHAM-VEH	SHAM-CIT	OBX-VEH	OBX-CIT	2W ANOVA		Fisher LSD
RdHIPP							
Cho/NAA	0.195 ± *0.009*	0.192 ± *0.009*	0.195 ± *0.006*	0.192 ± *0.004*	OBX: F(1,38)=0.00, p=0.998	n.s.	N/A
					CIT: F(1,38)=0.27, p=0.606	n.s.	N/A
					OBX*CIT: F(1,38)=0.00, p=0.993	n.s.	N/A
Cho/tCr	0.164 ± *0.005*	0.155 ± *0.006*	0.154 ± *0.005*	0.152 ± *0.005*	OBX: F(1,38)=1.60, p=0.214	n.s.	N/A
					CIT: F(1,38)=1.10, p=0.300	n.s.	N/A
					OBX*CIT: F(1,38)=0.35, p=0.559	n.s.	N/A
NAA/tCr	0.848 ± *0.032*	0.814 ± *0.017*	0.792 ± *0.024*	0.792 ± *0.024*	OBX: F(1,38)=2.20, p=0.146	n.s.	N/A
					CIT: F(1,38)=0.40, p=0.529	n.s.	N/A
					OBX*CIT: F(1,38)=0.44, p=0.509	n.s.	N/A
Glx/tCr	1.457 ± *0.030*	1.439 ± *0.032*	1.377 ± *0.027*	1.468 ± *0.041*	OBX: F(1,38)=0.53, p=0.473	n.s.	N/A
					CIT: F(1,38)=1.09, p=0.303	n.s.	N/A
					OBX*CIT: F(1,38)=2.44, p=0.126	n.s.	N/A
mI/tCr	0.704 ± *0.028*	0.622 ± *0.019*	0.645 ± *0.024*	0.691 ± *0.022*	OBX: F(1,38)=0.04, p=0.842	n.s.	N/A
					CIT: F(1,38)=0.55, p=0.462	n.s.	N/A
					OBX*CIT: F(1,38)=6.63, p=0.014	*	SHAM-VEH>SHAM-CIT*
Tau/tCr	0.677 ± *0.040*	0.617 ± *0.029*	0.665 ± *0.019*	0.616 ± *0.027*	OBX: F(1,38)=0.05, p=0.827	n.s.	N/A
					CIT: F(1,38)=3.16, p=0.084	n.s.	N/A
					OBX*CIT: F(1,38)=0.03, p=0.866	n.s.	N/A
Glu/tCr	0.933 ± *0.034*	0.963 ± *0.033*	0.904 ± *0.028*	0.946 ± *0.032*	OBX: F(1,38)=0.47, p=0.496	n.s.	N/A
					CIT: F(1,38)=1.13, p=0.294	n.s.	N/A
					OBX*CIT: F(1,38)=0.03, p=0.861	n.s.	N/A
Gln/tCr	0.524 ± *0.022*	0.476 ± *0.023*	0.473 ± *0.026*	0.522 ± *0.018*	OBX: F(1,38)=0.01, p=0.920	n.s.	N/A
					CIT: F(1,38)=0.00, p=0.964	n.s.	N/A
					OBX*CIT: F(1,38)=4.06, p=0.051	n.s.	N/A
LdHIPP							
Cho/NAA	0.192 ± *0.006*	0.192 ± *0.008*	0.188 ± *0.007*	0.190 ± *0.010*	OBX: F(1,38)=0.13, p=0.720	n.s.	N/A
					CIT: F(1,38)=0.02, p=0.886	n.s.	N/A
					OBX*CIT: F(1,38)=0.02, p=0.896	n.s.	N/A
Cho/tCr	0.162 ± *0.005*	0.162 ± *0.007*	0.151 ± *0.004*	0.145 ± *0.005*	OBX: F(1,38)=6.19, p=0.017	SHAM>OBX*	N/A
					CIT: F(1,38)=0.35, p=0.557	n.s.	N/A
					OBX*CIT: F(1,38)=0.36, p=0.553	n.s.	N/A
NAA/tCr	0.849 ± *0.030*	0.844 ± *0.019*	0.817 ± *0.031*	0.783 ± *0.042*	OBX: F(1,38)=1.78, p=0.190	n.s.	N/A
					CIT: F(1,38)=0.31, p=0.579	n.s.	N/A
					OBX*CIT: F(1,38)=0.18, p=0.676	n.s.	N/A
Glx/tCr	1.531 ± *0.037*	1.408 ± *0.033*	1.449 ± *0.049*	1.521 ± *0.041*	OBX: F(1,38)=0.11, p=0.738	n.s.	N/A
					CIT: F(1,38)=0.34, p=0.565	n.s.	N/A
					OBX*CIT: F(1,38)=4.84, p=0.034	*	n.s.
mI/tCr	0.838 ± *0.018*	0.742 ± *0.049*	0.791 ± *0.024*	0.797 ± *0.040*	OBX: F(1,38)=0.01, p=0.909	n.s.	N/A
					CIT: F(1,38)=1.58, p=0.217	n.s.	N/A
					OBX*CIT: F(1,38)=2.07, p=0.159	n.s.	N/A
Tau/tCr	0.783 ± *0.036*	0.750 ± *0.033*	0.803 ± *0.025*	0.714 ± *0.035*	OBX: F(1,38)=0.06, p=0.815	n.s.	N/A
					CIT: F(1,38)=3.22, p=0.081	n.s.	N/A
					OBX*CIT: F(1,38)=0.67, p=0.417	n.s.	N/A
Glu/tCr	0.963 ± *0.043*	0.926 ± *0.027*	0.939 ± *0.047*	0.994 ± *0.032*	OBX: F(1,38)=0.28, p=0.601	n.s.	N/A
					CIT: F(1,38)=0.04, p=0.837	n.s.	N/A
					OBX*CIT: F(1,38)=1.21, p=0.277	n.s.	N/A
Gln/tCr	0.568 ± *0.018*	0.482 ± *0.028*	0.509 ± *0.018*	0.527 ± *0.021*	OBX: F(1,38)=0.10, p=0.756	n.s.	N/A
					CIT: F(1,38)=2.34, p=0.135	n.s.	N/A
					OBX*CIT: F(1,38)=5.26, p=0.027	*	SHAM-VEH>SHAM-CIT*
dHIPP - averaged values							
Cho/NAA	0.194 ± *0.006*	0.192 ± *0.006*	0.192 ± *0.004*	0.191 ± *0.005*	OBX: F(1,38)=0.06, p=0.803	n.s.	N/A
					CIT: F(1,38)=0.06, p=0.810	n.s.	N/A
					OBX*CIT: F(1,38)=0.02, p=0.905	n.s.	N/A
Cho/tCr	0.163 ± *0.005*	0.158 ± *0.005*	0.153 ± *0.004*	0.148 ± *0.004*	OBX: F(1,38)=4.91, p=0.033	SHAM>OBX*	N/A
					CIT: F(1,38)=0.92, p=0.343	n.s.	N/A
					OBX*CIT: F(1,38)=0.00, p=0.989	n.s.	N/A
NAA/tCr	0.849 ± *0.024*	0.829 ± *0.015*	0.804 ± *0.024*	0.788 ± *0.028*	OBX: F(1,38)=2.79, p=0.103	n.s.	N/A
					CIT: F(1,38)=0.51, p=0.482	n.s.	N/A
					OBX*CIT: F(1,38)=0.00, p=0.952	n.s.	N/A
Glx/tCr	1.494 ± *0.026*	1.423 ± *0.018*	1.413 ± *0.033*	1.494 ± *0.030*	OBX: F(1,38)=0.03, p=0.858	n.s.	N/A
					CIT: F(1,38)=0.03, p=0.861	n.s.	N/A
					OBX*CIT: F(1,38)=6.35, p=0.016	*	n.s.
mI/tCr	0.771 ± *0.015*	0.682 ± *0.027*	0.718 ± *0.021*	0.744 ± *0.028*	OBX: F(1,38)=0.03, p=0.856	n.s.	N/A
					CIT: F(1,38)=1.63, p=0.209	n.s.	N/A
					OBX*CIT: F(1,38)=5.47, p=0.025	*	SHAM-VEH>SHAM-CIT*
Tau/tCr	0.730 ± *0.029*	0.684 ± *0.026*	0.734 ± *0.018*	0.665 ± *0.029*	OBX: F(1,38)=0.08, p=0.782	n.s.	N/A
					CIT: F(1,38)=4.51, p=0.040	VEH>CIT*	N/A
					OBX*CIT: F(1,38)=0.17, p=0.679	n.s.	N/A
Glu/tCr	0.948 ± *0.029*	0.944 ± *0.024*	0.922 ± *0.032*	0.970 ± *0.024*	OBX: F(1,38)=0.00, p=0.987	n.s.	N/A
					CIT: F(1,38)=0.54, p=0.468	n.s.	N/A
					OBX*CIT: F(1,38)=0.76, p=0.390	n.s.	N/A

(*continued on next page*)

Table 2 (*continued*)

	SHAM-VEH	SHAM-CIT	OBX-VEH	OBX-CIT	2W ANOVA		Fisher LSD
Gln/tCr	0.546 ± *0.018*	0.479 ± *0.015*	0.491 ± *0.016*	0.524 ± *0.015*	OBX: F(1,38)=0.08, p=0.777	n.s.	N/A
					CIT: F(1,38)=0.97, p=0.331	n.s.	N/A
					OBX*CIT: F(1,38)=8.86, p=0.005	**	SHAM-VEH>SHAM-CIT*
							SHAM-VEH>OBX-VEH*

The table summarises the means ± SEM of the metabolites' ratios together with details of the statistical analysis in both lateral regions and their average (*p<0.05, **p<0.01).

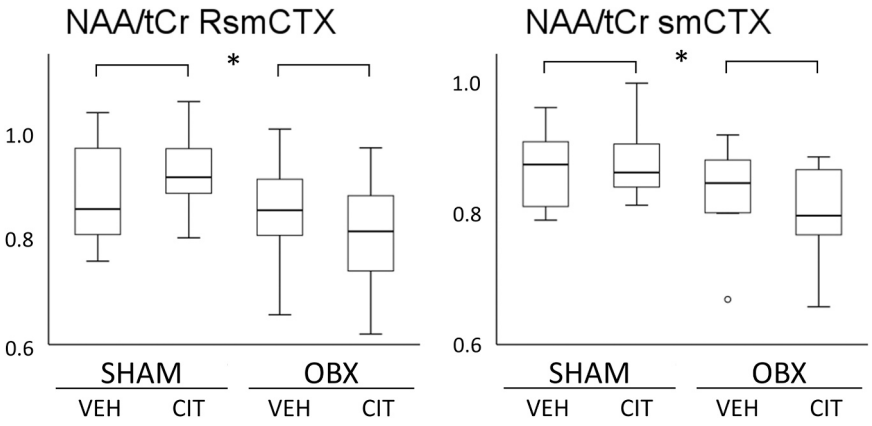

Fig. 6. : ^{1}H MRS results – sensorimotor cortex. The main effect of the OB model on relative metabolite concentration in the sensorimotor cortex. In the boxplots, the whiskers display the maximum and minimum values (except outliers - ○), top of the box is quartile 3, line inside the box is median, and bottom of the box is quartile 1 (*p<0.05, **p<0.01).

locomotor response. The forced-swim test demonstrated the effect of CIT, which increased swimming behaviour in both the SHAM and OBX groups, and reflects the serotonergic mechanism of the antidepressant [51,52]. The number of faecal boli in the locomotor apparatus indicated the effect of the OB model (more boli in the OBX groups) and the normalising effect of the chronic CIT treatment. Consequently, it can be concluded that the behavioural profile confirmed the successful development of an OB-induced phenotype, consistently observed in our laboratory [32,34,36], as well as the effect of the treatment.

4.1. Proton magnetic resonance spectroscopy findings

Regarding the primary OB model effect, the ^{1}H MRS results of this study partially corroborated our pilot study findings, which observed lower levels of Cho/NAA and Cho/tCr in the right dorsal hippocampus of the OBX rats [22]. In the current study a similar effect was observed in the left hemisphere. Therefore, the averaged ^{1}H MRS data from both hippocampi was also assessed and confirmed the finding of lower Cho/tCr. However, unlike in the pilot study, no difference in Cho/NAA levels was found. This may be a consequence of non-significantly lower levels of NAA in the left dorsal hippocampus of the OBX rats in this study, as it appears as a denominator in the metabolite ratio. It also may be attributed to a higher difference in Cho/tCr mean levels within the pilot *vs.* treatment studies. However, with respect to Cho/tCr levels, the OB model effect is more unequivocal, as a stable creatine level is expected, which is used as an internal reference [53]. As a lower level of Cho/tCr was found once in the right hippocampus in the pilot study, and subsequently in the left hippocampus and in the averaged values from both hemispheres in the current study, the OB model effect may be lateralized. Therefore, we propose assessing both sides of the bilateral brain structures, as well as the averaged values, to detect any potential difference. The OB model effect in Cho/tCr levels in the hippocampal regions may be attributed to disturbed memory function, as has been reported in MDD patients [26], and also as choline is a precursor of acetylcholine, which plays a significant role in memory storage [25]. Furthermore, these results correspond to other depression models: Cho/tCr reduction has been found in the forced-swim test model in the left dorsal hippocampus but not in the right one [54], and it was lower in both right and left hippocampi in the congenital learned helplessness model [55]. Therefore, it appears that hippocampal choline may be a biomarker for a depressive-like phenotype in rodents.

In the current dataset, the OB model exhibited lower NAA/tCr in the right sensorimotor cortex, and in the averaged values from both hemispheres. This finding was not observed in the pilot study, potentially due to insufficient cortical data quality and, consequently, a low number of analysed spectra from the sensorimotor cortex (n_{SHAM}=4, n_{OBX}=5). As NAA is considered a marker of functional neurons [53], the disparity between the model and control groups suggests neuronal dysfunction in the OB model animals. Lower NAA levels in the cortical regions have not been reported in any other rodent depression model [11]. Conversely, higher NAA has been observed in the prefrontal cortex in the chronic forced-swim stress model [56], and a delayed NAA increase was reported in the medial prefrontal cortex of the intermittent social defeat stress model [57]. This discrepancy may be attributed diverse voxel positioning, as in both studies, unlike in our experiments, white matter (*corpus callosum*) was included in the measured voxel. However, it also may be due to a different type of MDD model; surgical *vs.* stress-induced. Although the NAA results lack uniformity, we propose sensorimotor cortical NAA/tCr as a biomarker of the OB model, as it reflects the neuronal function which is altered in specific brain structures in human depression [58,59].

The main chronic citalopram treatment effect in the current study was shown only in the averaged dorsal hippocampus data, where Tau/tCr was lower in the CIT-treated rats than in the VEH-treated groups. Tau is considered an osmoregulator and a modulator of neurotransmitter actions, which may be pertinent to the pharmacodynamics of the drug. We consider a significant decrease in Tau/tCr level due to antidepressant treatment to be potentially detrimental, as taurine exhibits a neuroprotective function [60]. Furthermore, citalopram did not reverse the main OB model effect in the hippocampus or the cortex. Notably, in two studies of the congenital learned helplessness model Tau/tCr was higher in the right and the left dorsal hippocampus compared to the

Table 3
^{1}H MRS data from the sensorimotor cortex.

	SHAM-VEH	SHAM-CIT	OBX-VEH	OBX-CIT	2W ANOVA	
RsmCTX						
Cho/NAA	0.131 ± *0.007*	0.126 ± *0.003*	0.133 ± *0.007*	0.142 ± *0.007*	OBX: F(1,38)=1.61, p=0.212	n.s.
					CIT: F(1,38)=0.12, p=0.731	n.s.
					OBX*CIT: F(1,38)=1.05, p=0.313	n.s.
Cho/tCr	0.115 ± *0.004*	0.117 ± *0.003*	0.112 ± *0.005*	0.114 ± *0.005*	OBX: F(1,38)=0.30, p=0.589	n.s.
					CIT: F(1,38)=0.18, p=0.673	n.s.
					OBX*CIT: F(1,38)=0.00, p=0.960	n.s.
NAA/tCr	0.885 ± *0.029*	0.929 ± *0.027*	0.854 ± *0.025*	0.811 ± *0.033*	OBX: F(1,38)=5.98, p=0.019	SHAM>OBX*
					CIT: F(1,38)=0.00, p=0.987	n.s.
					OBX*CIT: F(1,38)=2.00, p=0.165	n.s.
Glx/tCr	1.351 ± *0.051*	1.402 ± *0.038*	1.400 ± *0.045*	1.306 ± *0.046*	OBX: F(1,38)=0.24, p=0.629	n.s.
					CIT: F(1,38)=0.20, p=0.658	n.s.
					OBX*CIT: F(1,38)=2.25, p=0.142	n.s.
mI/tCr	0.418 ± *0.043*	0.438 ± *0.033*	0.404 ± *0.050*	0.363 ± *0.038*	OBX: F(1,38)=0.96, p=0.334	n.s.
					CIT: F(1,38)=0.05, p=0.821	n.s.
					OBX*CIT: F(1,38)=0.47, p=0.496	n.s.
Tau/tCr	0.661 ± *0.030*	0.667 ± *0.024*	0.666 ± *0.035*	0.669 ± *0.041*	OBX: F(1,38)=0.01, p=0.926	n.s.
					CIT: F(1,38)=0.01, p=0.906	n.s.
					OBX*CIT: F(1,38)=0.00, p=0.978	n.s.
Glu/tCr	0.929 ± *0.025*	0.967 ± *0.044*	0.943 ± *0.048*	0.899 ± *0.035*	OBX: F(1,38)=0.42, p=0.521	n.s.
					CIT: F(1,38)=0.00, p=0.950	n.s.
					OBX*CIT: F(1,38)=0.93, p=0.341	n.s.
Gln/tCr	0.421 ± *0.037*	0.434 ± *0.021*	0.457 ± *0.032*	0.407 ± *0.030*	OBX: F(1,38)=0.01, p=0.907	n.s.
					CIT: F(1,38)=0.33, p=0.571	n.s.
					OBX*CIT: F(1,38)=0.92, p=0.344	n.s.
LsmCTX						
Cho/NAA	0.141 ± *0.006*	0.137 ± *0.007*	0.140 ± *0.004*	0.159 ± *0.009*	OBX: F(1,34)=2.22, p=0.145	n.s.
					CIT: F(1,34)=1.28, p=0.266	n.s.
					OBX*CIT: F(1,34)=2.78, p=0.105	n.s.
Cho/tCr	0.119 ± *0.005*	0.114 ± *0.005*	0.114 ± *0.003*	0.119 ± *0.003*	OBX: F(1,34)=0.01, p=0.919	n.s.
					CIT: F(1,34)=0.01, p=0.922	n.s.
					OBX*CIT: F(1,34)=1.58, p=0.217	n.s.
NAA/tCr	0.847 ± *0.025*	0.836 ± *0.030*	0.818 ± *0.020*	0.767 ± *0.034*	OBX: F(1,34)=2.83, p=0.102	n.s.
					CIT: F(1,34)=1.15, p=0.292	n.s.
					OBX*CIT: F(1,34)=0.44, p=0.512	n.s.
Glx/tCr	1.398 ± *0.056*	1.351 ± *0.052*	1.370 ± *0.033*	1.349 ± *0.032*	OBX: F(1,34)=0.11, p=0.745	n.s.
					CIT: F(1,34)=0.53, p=0.471	n.s.
					OBX*CIT: F(1,34)=0.09, p=0.772	n.s.
mI/tCr	0.360 ± *0.025*	0.365 ± *0.029*	0.367 ± *0.020*	0.341 ± *0.026*	OBX: F(1,34)=0.10, p=0.750	n.s.
					CIT: F(1,34)=0.15, p=0.701	n.s.
					OBX*CIT: F(1,34)=0.34, p=0.561	n.s.
Tau/tCr	0.598 ± *0.020*	0.540 ± *0.030*	0.628 ± *0.023*	0.579 ± *0.031*	OBX: F(1,34)=1.56, p=0.220	n.s.
					CIT: F(1,34)=3.79, p=0.060	n.s.
					OBX*CIT: F(1,34)=0.03, p=0.872	n.s.
Glu/tCr	0.973 ± *0.051*	0.922 ± *0.040*	0.915 ± *0.026*	0.932 ± *0.025*	OBX: F(1,34)=0.39, p=0.538	n.s.
					CIT: F(1,34)=0.18, p=0.677	n.s.
					OBX*CIT: F(1,34)=0.77, p=0.387	n.s.
Gln/tCr	0.425 ± *0.016*	0.428 ± *0.023*	0.455 ± *0.029*	0.417 ± *0.017*	OBX: F(1,34)=0.16, p=0.691	n.s.
					CIT: F(1,34)=0.57, p=0.456	n.s.
					OBX*CIT: F(1,34)=0.82, p=0.372	n.s.
smCTX - averaged values						
Cho/NAA	0.136 ± *0.005*	0.131 ± *0.005*	0.135 ± *0.003*	0.147 ± *0.005*	OBX: F(1,34)=2.41, p=0.130	n.s.
					CIT: F(1,34)=0.54, p=0.466	n.s.
					OBX*CIT: F(1,34)=2.81, p=0.103	n.s.
Cho/tCr	0.117 ± *0.004*	0.115 ± *0.003*	0.110 ± *0.003*	0.116 ± *0.003*	OBX: F(1,34)=0.60, p=0.446	n.s.
					CIT: F(1,34)=0.41, p=0.526	n.s.
					OBX*CIT: F(1,34)=1.46, p=0.235	n.s.
NAA/tCr	0.866 ± *0.019*	0.879 ± *0.021*	0.821 ± *0.020*	0.808 ± *0.023*	OBX: F(1,34)=7.18, p=0.011	SHAM>OBX*
					CIT: F(1,34)=0.00, p=1.000	n.s.
					OBX*CIT: F(1,34)=0.35, p=0.558	n.s.
Glx/tCr	1.375 ± *0.030*	1.365 ± *0.025*	1.355 ± *0.027*	1.309 ± *0.036*	OBX: F(1,34)=1.34, p=0.255	n.s.
					CIT: F(1,34)=0.77, p=0.387	n.s.
					OBX*CIT: F(1,34)=0.32, p=0.574	n.s.
mI/tCr	0.389 ± *0.023*	0.409 ± *0.010*	0.391 ± *0.022*	0.366 ± *0.026*	OBX: F(1,34)=0.75, p=0.391	n.s.
					CIT: F(1,34)=0.01, p=0.921	n.s.
					OBX*CIT: F(1,34)=0.94, p=0.339	n.s.
Tau/tCr	0.630 ± *0.019*	0.601 ± *0.024*	0.628 ± *0.023*	0.613 ± *0.023*	OBX: F(1,34)=0.05, p=0.820	n.s.
					CIT: F(1,34)=0.85, p=0.364	n.s.
					OBX*CIT: F(1,34)=0.09, p=0.770	n.s.
Glu/tCr	0.951 ± *0.030*	0.931 ± *0.024*	0.911 ± *0.025*	0.909 ± *0.025*	OBX: F(1,34)=1.22, p=0.277	n.s.
					CIT: F(1,34)=0.17, p=0.683	n.s.
					OBX*CIT: F(1,34)=0.11, p=0.744	n.s.
Gln/tCr	0.423 ± *0.019*	0.434 ± *0.013*	0.444 ± *0.014*	0.400 ± *0.022*	OBX: F(1,34)=0.12, p=0.733	n.s.
					CIT: F(1,34)=0.79, p=0.381	n.s.
					OBX*CIT: F(1,34)=2.11, p=0.156	n.s.

The table summarises the means ± SEM of the metabolites' ratios together with details of the statistical analysis in both lateral regions and their average (*p<0.05).

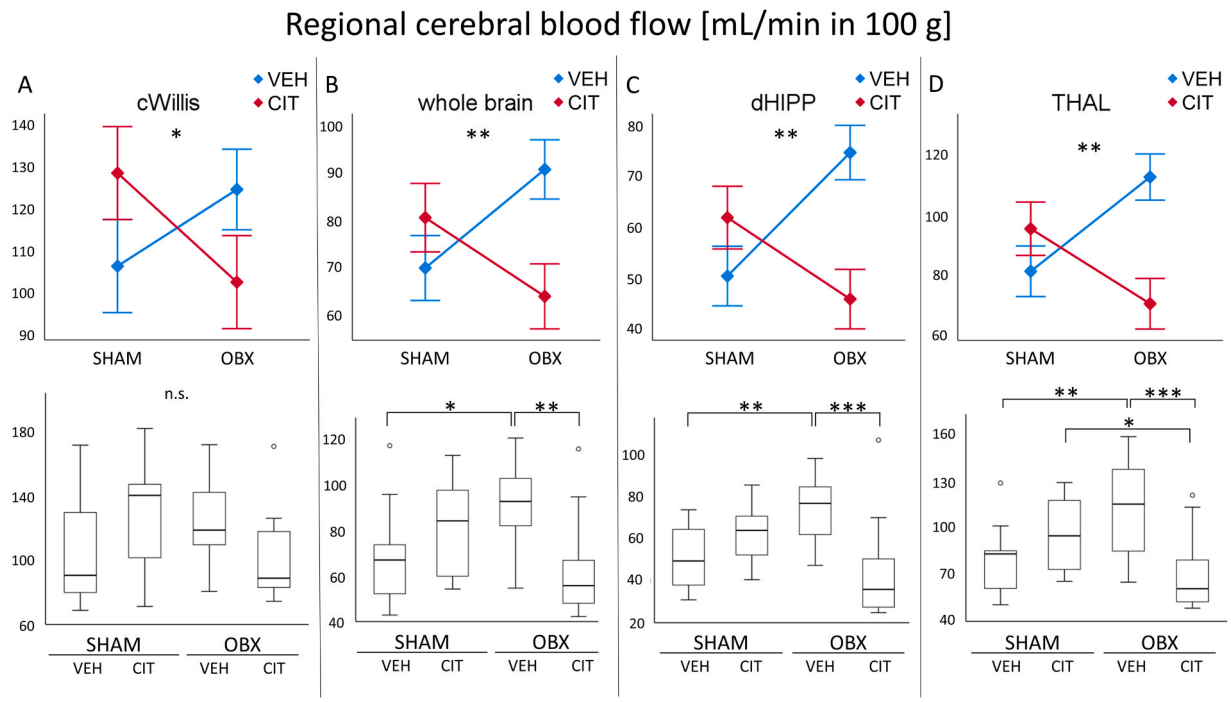

Fig. 7. : rCBF results. A-D – top parts show the interactions of the study's main effects: OB model-citalopram treatment on regional cerebral blood flow. A-D – bottom parts show the group differences revealed by the LSD post-hoc test. In the boxplots, the whiskers display the maximum and minimum values (except outliers - ○), top of the box is quartile 3, line inside the box is median, and bottom of the box is quartile 1 (*p<0.05, **p<0.01, ***p<0.001).

controls [55,61], therefore citalopram treatment may reverse this phenotype in the model. Additionally, in Biedermann's study [61], Tau/tCr was lowered by electroconvulsive therapy but not by clomipramine treatment. No similar treatment effects have been observed in the depression rodent models thus far [11]. Therefore, if we consider Tau as a hippocampal biomarker of a depressive-like phenotype, the OB model does not replicate this notion. A study utilizing escitalopram treatment in an unpredictable chronic mild stress model demonstrated partial reversal of lower NAA/tCr in the right dorsal hippocampus [62]. However, in our results, there was no hippocampal NAA alteration, nor did the citalopram treatment affect hippocampal NAA levels. NAA was shown to be lower in the cortex of the OBX rats; however, citalopram demonstrated no effect in this region.

The OB model–citalopram treatment interaction revealed using ^{1}H MRS was significant only in the hippocampal regions, particularly in mI/tCr, Gln/tCr and Glx/tCr. It can be inferred that Glx was present due to Gln, as Glx=Glu+Gln, however there was no group difference in a post-hoc test. In mI/tCr and Gln/tCr, the OB model-citalopram treatment interaction yielded the same result: metabolite ratio levels were significantly higher in the sham-operated vehicle-treated group than in the sham-operated citalopram-treated group. In the OBX groups, the effect of the CIT treatment exhibited an opposite trend, although post-hoc testing did not reveal a significant group difference. These results suggest a differential treatment effect on the OBX *vs.* SHAM groups while significantly affecting only the control animals: reducing mI/tCr and Gln/tCr. Altered mI and Gln levels indicate a change in the quantity of glial cells, as both metabolites are considered glial cell markers [53]. The relationship between glial cells and depression was assessed by Rial et al. [63] who reported that the decreased astrocytes' function may cause depressive (in animals depressive-like) symptoms. Therefore, it can be concluded that the chronic CIT treatment had a detrimental effect on the rats, while in the OB model group it did not exert a significant alteration. However, as the results indicate, a potentially beneficial effect in the model rats may be anticipated despite the insignificant post-hoc analysis.

4.2. *Regional cerebral blood flow findings*

The rCBF data in this study provide limited scope for discussion, and in general there is a paucity of data from perfusion studies exploring rodent MDD models. In this study, no main effects of the OB model and the citalopram treatment were observed, but differential effects of the CIT treatment in the OB model and control rats were noted. Specifically, in the dorsal hippocampus, thalamus and the whole brain, higher rCBF was found in the OBX rats, which was normalised by the citalopram treatment, with no significant effect on the control rats. No OB model effect was found in our previous pilot study [22] or in another OB study by Gigliucci et al. [23]. Also, one recent study reported no difference in hippocampal CBF in forced swim MDD model [24]. Furthermore, reduced rCBF was demonstrated in the cortical and striatal regions in the Wistar-Kyoto rat MDD model, while no effect was shown in the thalamus [64], and there was reduced regional cerebral blood volume in the congenital learned helplessness depression model, particularly in the habenular structures, dentate gyrus and subiculum [65]. These conflicting outcomes indicate the specificity of the perfusion NMR markers on the MDD phenotypes [66] and on different types of MDD. However, a pattern of replicable rCBF alterations in the depressive-like phenotype is yet to be identified. One key challenge for the reproducibility of perfusion data may lie in the data processing. To address this, we optimised the delineation of the regions of interest in this study by following up with correction on perfusion maps. This advanced approach enabled us to avoid including large vessels in the investigated region, which may alter the rCBF estimates. Consequently, the improved data processing may have facilitated the identification of the differential effects of citalopram treatment in the SHAM and OB groups.

Regarding the treatment effect of citalopram, the higher perfusion in the OBX-VEH rats in the dorsal hippocampus, thalamus and whole brain was normalized by citalopram in the OBX-CIT group, while unaffecting the SHAM group. This finding is noteworthy, and to the best of our knowledge, no data demonstrate a similar phenomenon in animal models of depression. Normalisation of rCBF changes in depression was observed repeatedly in small clinical trials in MDD patients who

Table 4
rCBF data in the examined brain regions.

rCBF	SHAM-VEH	SHAM-CIT	OBX-VEH	OBX-CIT	2 W ANOVA		Fisher LSD
Circle of Willis	106.64 ± *11.58*	128.63 ± *11.87*	124.75 ± *7.45*	102.85 ± *9.80*	OBX: F(1,35)=0.13, p=0.721	n.s.	N/A
					CIT: F(1,35)=0.00, p=0.997	n.s.	N/A
					OBX*CIT: F(1,35)=4.25, p=0.047	*	n.s.
Whole brain	69.83 ± *6.64*	80.46 ± *6.78*	90.65 ± *5.41*	63.84 ± *7.12*	OBX: F(1,37)=0.09, p=0.760	n.s.	N/A
					CIT: F(1,37)=1.41, p=0.243	n.s.	N/A
					OBX*CIT: F(1378)=7.54, p=0.009	**	OBX-VEH>SHAM-VEH*
							OBX-VEH>OBX-CIT**
smCTX	63.69 ± *7.55*	64.10 ± *5.11*	74.75 ± *5.64*	55.29 ± *7.02*	OBX: F(1,37)=0.03, p=0.869	n.s.	N/A
					CIT: F(1,37)=1.96, p=0.169	n.s.	N/A
					OBX*CIT: F(1,37)=2.14, p=0.152	n.s.	N/A
pirCTX	87.47 ± *6.80*	91.49 ± *9.86*	83.21 ± *4.13*	79.77 ± *6.52*	OBX: F(1,37)=1.25, p=0.272	n.s.	N/A
					CIT: F(1,37)=0.00, p=0.968	n.s.	N/A
					OBX*CIT: F(1,37)=0.27, p=0.605	n.s.	N/A
HIPP	50.38 ± *4.44*	61.85 ± *4.74*	74.61 ± *4.49*	45.86 ± *7.70*	OBX: F(1,37)=0.50, p=0.482	n.s.	N/A
					CIT: F(1,37)=2.22, p=0.145	n.s.	N/A
					OBX*CIT: F(1,37)=12.03, p=0.001	**	OBX-VEH>SHAM-VEH**
							OBX-VEH>OBX-CIT***
THAL	81.38 ± *6.87*	95.56 ± *7.60*	112.76 ± *8.58*	70.59 ± *7.90*	OBX: F(1,37)=0.15, p=0.703	n.s.	N/A
					CIT: F(1,37)=2.80, p=0.103	n.s.	N/A
					OBX*CIT: F(1,37)=11.35, p=0.002	**	OBX-VEH>SHAM-VEH**
							SHAM-CIT>OBX-CIT*
							OBX-VEH>OBX-CIT***

The table summarises the means ± SEM of the regional cerebral blood flow together with details of the statistical analysis (*p<0.05, **p<0.01, ***p<0.001).

exhibited rCBF changes (both higher and lower perfusion compared to healthy controls), which were normalised by chronic tricyclic antidepressant amitriptyline [67], escitalopram [68] or citalopram [69] treatment. Therefore, there appears to be some evidence of antidepressant-induced normalisation of rCBF in MDD. Unfortunately, clinical trials rarely include healthy patient groups receiving the treatment, thus precluding verification of whether the treatment effect is dependent or independent of the condition. One exception is a trial which examined paroxetine (an SSRI antidepressant like citalopram) and reported a rCBF decrease in multiple brain regions in healthy human volunteers after 7 days of treatment [70]. Furthermore, ecstasy, a predominantly indirect serotonergic enhancer, exerted an attenuation of rCBF after repeated administration in prefrontal regions but not in the thalamus [71].

There is also evidence of rCBF changes following acute citalopram treatment. A decrease in blood flow in several anatomically and functionally diverse regions, not including the thalamus, was reported in an *ex vivo* autoradiographic study in rats [72]. Clinically, the acute effect of citalopram was examined in healthy volunteers, demonstrating an increase in thalamic CBF [73]. However, a citalopram-induced reduction in CBF in the amygdala, fusiform gyrus, insula, hippocampus, orbitofrontal cortex, pulvinar nucleus and hypothalamus was also reported [74–76]. Although the findings in the thalamus in these studies and the current study are contradictory, and the relevance of an acute effect in a discussion of chronic exposure effects is largely limited, citalopram has consistently been shown to be capable of altering brain haemodynamics after acute and chronic treatment in experimental animals and humans.

5. Conclusion

This study examined the olfactory bulbectomy model effect, the citalopram treatment effect and their interaction in relation to the neurochemical profile of the brain and regional cerebral blood flow in rats. ^{1}H MRS detected key brain metabolite differences in the OB model, and we suggest Cho/tCr as an OB phenotype biomarker in the hippocampus, and NAA/tCr in the sensorimotor cortex. Furthermore, the citalopram treatment exhibited potentially deleterious effects, as it caused Tau/tCr reduction, which indicates impaired osmoregulation, and modulation of neurotransmitter actions and neuroprotection. Citalopram did not normalise the main OB phenotype effect in the neurochemical profile of the hippocampus and sensorimotor cortex. The interaction of the OB model and the citalopram treatment demonstrated a potentially harmful effect of citalopram in the control rats, as fewer glia were observed in the hippocampus of the citalopram-treated controls. However, citalopram also indicated a beneficial effect as the glia in the depressive-like phenotype seemed to be increased. A normalising citalopram effect was present in the perfusion experiment as citalopram normalised higher perfusion in the hippocampus, thalamus and the whole brain in the OB rats without affecting the control rats. Despite the established clinical efficacy of citalopram, there are two unremedied OB-induced traits, hippocampal Cho/tCr and cortical NAA/tCr. Their clinical relevance is yet to be determined, however they may become future markers of highly effective antidepressants. The NMR technique appears to be an appropriate tool for such research, as the ^{1}H MRS approach proved its capacity to capture an OB-induced phenotype and chronic antidepressant treatment effects, while both functional NMR methods found an OB model-citalopram treatment interaction showing a different effect of the antidepressant on the control *vs.* depressive-like rat brain.

Funding

The study performed at Masaryk University was part of the project "Preclinical and clinical research of the Institute of Pharmacology in the field of biotransformation of drugs, behavioural neuropsychopharmacology and personalised pharmacotherapy in oncology" number MUNI/A/1580/2023, with the support of the Specific University Research Grant, as provided by the Ministry of Education, Youth and Sports of the Czech Republic (MEYS CR) in the year 2024. All NMR experiments and data analysis were carried out by the ISI-MR facility of the Czech-BioImaging infrastructure, supported by grants LM2018129 and LM2023050 of the MEYS CR and GA22–10953S supported by the Czech Science Foundation.

CRediT authorship contribution statement

Jiri Vitous: Writing – review & editing, Methodology, Investigation. **Radovan Jirik:** Writing – review & editing, Supervision, Methodology, Investigation. **Jana Ruda-Kucerova:** Writing – review & editing, Visualization, Supervision, Methodology, Investigation, Formal analysis, Data curation, Conceptualization. **Ondrej Macicek:** Writing – review & editing, Methodology, Investigation. **Petra Amchova:** Writing –

review & editing, Methodology, Investigation. **Maria Hrickova:** Writing – review & editing, Methodology, Investigation. **Iveta Harastova-Pavlova:** Writing – review & editing, Writing – original draft, Visualization, Methodology, Investigation, Formal analysis, Data curation, Conceptualization. **Eva Drazanova:** Writing – review & editing, Methodology, Investigation, Data curation. **Lucie Kratka:** Writing – review & editing, Methodology, Investigation.

Declaration of Competing Interest

The authors declare no conflict of interest.

Acknowledgements

We are grateful to Ing. Zenon Starčuk jr., CSc., for supporting our NMR research, sharing knowledge and providing encouragement and financial support. Professional language editing was performed by Michelle Burke.

References

[1] S. Shorey, E.D. Ng, C.H.J. Wong, Global prevalence of depression and elevated depressive symptoms among adolescents: A systematic review and meta-analysis, Br. J. Clin. Psychol. 61 (2022) 287–305, https://doi.org/10.1111/bjc.12333.

[2] N. Abdoli, N. Salari, N. Darvishi, S. Jafarpour, M. Solaymani, M. Mohammadi, S. Shohaimi, The global prevalence of major depressive disorder (MDD) among the elderly: a systematic review and meta-analysis, Neurosci. Biobehav. Rev. 132 (2022) 1067–1073, https://doi.org/10.1016/j.neubiorev.2021.10.041.

[3] D.F. Santomauro, A.M. Mantilla Herrera, J. Shadid, P. Zheng, C. Ashbaugh, D. M. Pigott, C. Abbafati, C. Adolph, J.O. Amlag, A.Y. Aravkin, B.L. Bang-Jensen, G. J. Bertolacci, S.S. Bloom, R. Castellano, E. Castro, S. Chakrabarti, J. Chattopadhyay, R.M. Cogen, J.K. Collins, X. Dai, W.J. Dangel, C. Dapper, A. Deen, M. Erickson, S.B. Ewald, A.D. Flaxman, J.J. Frostad, N. Fullman, J. R. Giles, A.Z. Giref, G. Guo, J. He, M. Helak, E.N. Hulland, B. Idrisov, A. Lindstrom, E. Linebarger, P.A. Lotufo, R. Lozano, B. Magistro, D.C. Malta, J.C. Månsson, F. Marinho, A.H. Mokdad, L. Monasta, P. Naik, S. Nomura, J.K. O'Halloran, S. M. Ostroff, M. Pasovic, L. Penberthy, R.C. Reiner Jr, G. Reinke, A.L.P. Ribeiro, A. Sholokhov, R.J.D. Sorensen, E. Varavikova, A.T. Vo, R. Walcott, S. Watson, C. S. Wiysonge, B. Zigler, S.I. Hay, T. Vos, C.J.L. Murray, H.A. Whiteford, A.J. Ferrari, Global prevalence and burden of depressive and anxiety disorders in 204 countries and territories in 2020 due to the COVID-19 pandemic, Lancet 398 (2021) 1700–1712, https://doi.org/10.1016/S0140-6736(21)02143-7.

[4] S.C. Iancu, Y.M. Wong, D. Rhebergen, A.J.L.M. Van Balkom, N.M. Batelaan, Long-term disability in major depressive disorder: a 6-year follow-up study, Psychol. Med. 50 (2020) 1644–1652, https://doi.org/10.1017/S0033291719001612.

[5] S.H. Kennedy, Core symptoms of major depressive disorder: relevance to diagnosis and treatment, Dialog-. Clin. Neurosci. 10 (2008) 271–277, https://doi.org/10.31887/DCNS.2008.10.3/shkennedy.

[6] M.F. Steger, T.B. Kashdan, Depression and everyday social activity, belonging, and well-being, J. Couns. Psychol. 56 (2009) 289–300, https://doi.org/10.1037/a0015416.

[7] K.P. Ebmeier, J.T.O. Cavanagh, A.P.R. Moffoot, M.F. Glabus, R.E. O'Carroll, G. M. Goodwin, Cerebral perfusion correlates of depressed mood, Br. J. Psychiatry 170 (1997) 77–81, https://doi.org/10.1192/bjp.170.1.77.

[8] S. Moriguchi, A. Takamiya, Y. Noda, N. Horita, M. Wada, S. Tsugawa, E. Plitman, Y. Sano, R. Tarumi, M. ElSalhy, N. Katayama, K. Ogyu, T. Miyazaki, T. Kishimoto, A. Graff-Guerrero, J.H. Meyer, D.M. Blumberger, Z.J. Daskalakis, M. Mimura, S. Nakajima, Glutamatergic neurometabolite levels in major depressive disorder: a systematic review and meta-analysis of proton magnetic resonance spectroscopy studies, Mol. Psychiatry 24 (2019) 952–964, https://doi.org/10.1038/s41380-018-0252-9.

[9] D.K. Rohra, Y. Qazi, Reliability of Rodent Models, in: P.M. Conn (Ed.), Sourceb. Models Biomed. Res., Humana Press, Totowa, NJ, 2008, pp. 213–217, https://doi.org/10.1007/978-1-59745-285-4_24.

[10] Q. Wang, M.A. Timberlake, K. Prall, Y. Dwivedi, The recent progress in animal models of depression, Prog. Neuropsychopharmacol. Biol. Psychiatry 77 (2017) 99–109, https://doi.org/10.1016/j.pnpbp.2017.04.008.

[11] I. Pavlova, J. Ruda-Kucerova, Brain metabolic derangements examined using 1H MRS and their (in)consistency among different rodent models of depression, Prog. Neuropsychopharmacol. Biol. Psychiatry 127 (2023) 110808, https://doi.org/10.1016/j.pnpbp.2023.110808.

[12] D. Chaudhury, H. Liu, M.-H. Han, Neuronal correlates of depression, Cell. Mol. Life Sci. 72 (2015) 4825–4848, https://doi.org/10.1007/s00018-015-2044-6.

[13] R.S. Duman, Neuronal damage and protection in the pathophysiology and treatment of psychiatric illness: stress and depression, Dialog-. Clin. Neurosci. 11 (2009) 239–255, https://doi.org/10.31887/DCNS.2009.11.3/rsduman.

[14] C.-H. Lee, F. Giuliani, The role of inflammation in depression and fatigue, Front. Immunol. 10 (2019) 1696, https://doi.org/10.3389/fimmu.2019.01696.

[15] O. Bonne, Y. Krausz, Pathophysiological significance of cerebral perfusion abnormalities in major depression-trait or state marker? Eur. Neuropsychopharmacol. 7 (1997) 225–233, https://doi.org/10.1016/S0924-977X(97)00410-0.

[16] C.M. Cooper, C.R. Chin Fatt, P. Liu, B.D. Grannemann, T. Carmody, J.R.C. Almeida, T. Deckersbach, M. Fava, B.T. Kurian, A.L. Malchow, P.J. McGrath, M. McInnis, M. A. Oquendo, R.V. Parsey, E. Bartlett, M. Weissman, M.L. Phillips, H. Lu, M. H. Trivedi, Discovery and replication of cerebral blood flow differences in major depressive disorder, Mol. Psychiatry 25 (2020) 1500–1510, https://doi.org/10.1038/s41380-019-0464-7.

[17] S. Haller, G. Zaharchuk, D.L. Thomas, K.-O. Lovblad, F. Barkhof, X. Golay, Arterial spin labeling perfusion of the brain: emerging clinical applications, Radiology 281 (2016) 337–356, https://doi.org/10.1148/radiol.2016150789.

[18] Z. He, W. Sheng, F. Lu, Z. Long, S. Han, Y. Pang, Y. Chen, W. Luo, Y. Yu, X. Nan, Q. Cui, H. Chen, Altered resting-state cerebral blood flow and functional connectivity of striatum in bipolar disorder and major depressive disorder, Prog. Neuropsychopharmacol. Biol. Psychiatry 90 (2019) 177–185, https://doi.org/10.1016/j.pnpbp.2018.11.009.

[19] Y. Wang, Z. Yang, Aberrant pattern of cerebral blood flow in patients with major depressive disorder: a meta-analysis of arterial spin labelling studies, Psychiatry Res. Neuroimaging 321 (2022) 111458, https://doi.org/10.1016/j.pscychresns.2022.111458.

[20] S.J. Colloby, M.J. Firbank, J. He, A.J. Thomas, A. Vasudev, S.W. Parry, J.T. O'Brien, Regional cerebral blood flow in late-life depression: arterial spin labelling magnetic resonance study, Br. J. Psychiatry 200 (2018) 150–155, https://doi.org/10.1192/bjp.bp.111.092387.

[21] N. Weiduschat, M.J. Dubin, Prefrontal cortical blood flow predicts response of depression to rTMS, J. Affect. Disord. 150 (2013) 699–702, https://doi.org/10.1016/j.jad.2013.04.049.

[22] I. Pavlova, E. Drazanova, L. Kratka, P. Amchova, O. Macicek, J. Starcukova, Z. Starcuk, J. Ruda-Kucerova, Laterality in functional and metabolic state of the bulbectomised rat brain detected by ASL and ^{1}H MRS: a pilot study, World J. Biol. Psychiatry 24 (2023) 414–428, https://doi.org/10.1080/15622975.2022.2124450.

[23] V. Gigliucci, S. Gormley, S. Gibney, J. Rouine, C. Kerskens, T.J. Connor, A. Harkin, Characterisation of the antidepressant properties of nitric oxide synthase inhibitors in the olfactory bulbectomised rat model of depression, Eur. Neuropsychopharmacol. 24 (2014) 1349–1361, https://doi.org/10.1016/j.euroneuro.2014.05.003.

[24] D. Lee, C.-W. Woo, H. Heo, Y. Ko, J.S. Jang, S. Na, N. Kim, D.-C. Woo, K.W. Kim, D.-W. Lee, Mapping changes in glutamate with glutamate-weighted MRI in forced swim test model of depression in rats, Biomedicines 12 (2024) 384, https://doi.org/10.3390/biomedicines12020384.

[25] K. Löffelholz, J. Klein, A. Köppen, Chapter 23: Choline, a precursor of acetylcholine and phospholipids in the brain. Prog. Brain Res., Elsevier, 1993, pp. 197–200, https://doi.org/10.1016/S0079-6123(08)62399-7.

[26] G. Ende, D.F. Braus, S. Walter, W. Weber-Fahr, F.A. Henn, The hippocampus in patients treated with electroconvulsive therapy: a proton magnetic resonance spectroscopic imaging study, Arch. Gen. Psychiatry 57 (2000) 937, https://doi.org/10.1001/archpsyc.57.10.937.

[27] C. Song, B.E. Leonard, The olfactory bulbectomised rat as a model of depression, Neurosci. Biobehav. Rev. 29 (2005) 627–647, https://doi.org/10.1016/j.neubiorev.2005.03.010.

[28] F. Darcet, A. Gardier, R. Gaillard, D. David, J.-P. Guilloux, Cognitive dysfunction in major depressive disorder. a translational review in animal models of the disease, Pharmaceuticals 9 (2016) 9, https://doi.org/10.3390/ph9010009.

[29] Z. Babinska, J. Ruda-Kucerova, P. Amchova, J. Merhautova, L. Dusek, A. Sulcova, Olfactory bulbectomy increases reinstatement of methamphetamine seeking after a forced abstinence in rats, Behav. Brain Res. 297 (2016) 20–27, https://doi.org/10.1016/j.bbr.2015.09.035.

[30] Z. Babinska, J. Ruda-Kucerova, Differential characteristics of ketamine self-administration in the olfactory bulbectomy model of depression in male rats, Exp. Clin. Psychopharmacol. 25 (2017) 84–93, https://doi.org/10.1037/pha0000106.

[31] L. Fattore, P. Amchova, P. Fadda, J. Ruda-Kucerova, Olfactory bulbectomy model of depression lowers responding for food in male and female rats: the modulating role of caloric restriction and response requirement, Biomedicines 11 (2023) 2481, https://doi.org/10.3390/biomedicines11092481.

[32] J. Ruda-Kucerova, P. Amchova, T. Havlickova, P. Jerabek, Z. Babinska, P. Kacer, K. Syslova, A. Sulcova, M. Sustkova-Fiserova, Reward related neurotransmitter changes in a model of depression: An in vivo microdialysis study, World J. Biol. Psychiatry 16 (2015) 521–535, https://doi.org/10.3109/15622975.2015.1077991.

[33] J. Ruda-Kucerova, M.T. Zanda, P. Amchova, W. Fratta, L. Fattore, Sex and feeding status differently affect natural reward seeking behavior in olfactory bulbectomized rats, Front. Behav. Neurosci. 12 (2018) 255, https://doi.org/10.3389/fnbeh.2018.00255.

[34] F. Siska, P. Amchova, D. Kuruczova, Y. Tizabi, J. Ruda-Kucerova, Effects of low-dose alcohol exposure in adolescence on subsequent alcohol drinking in adulthood in a rat model of depression, World J. Biol. Psychiatry 22 (2021) 757–769, https://doi.org/10.1080/15622975.2021.1907717.

[35] J.P. Kelly, A.S. Wrynn, B.E. Leonard, The olfactory bulbectomized rat as a model of depression: an update, Pharmacol. Ther. 74 (1997) 299–316, https://doi.org/10.1016/S0163-7258(97)00004-1.

[36] P. Amchova, J. Ruda-Kucerova, Depressive-like phenotype enhances relapse of nicotine seeking after forced abstinence in rats, World J. Biol. Psychiatry 24 (2023) 46–57, https://doi.org/10.1080/15622975.2022.2070665.

[37] J. Ruda-Kucerova, Z. Babinska, M. Luptak, B. Getachew, Y. Tizabi, Both ketamine and NBQX attenuate alcohol drinking in male Wistar rats, Neurosci. Lett. 666 (2018) 175–180, https://doi.org/10.1016/j.neulet.2017.12.055.
[38] J. Ruda-Kucerova, J. Pistovcakova, P. Amchova, A. Sulcova, A. Machalova, Prenatal exposure to modafinil alters behavioural response to methamphetamine in adult male mice, Int. J. Dev. Neurosci. 67 (2018) 37–45, https://doi.org/10.1016/j.ijdevneu.2018.03.005.
[39] J. Ruda-Kucerova, Z. Babinska, T. Stark, V. Micale, Suppression of methamphetamine self-administration by ketamine pre-treatment is absent in the methylazoxymethanol (MAM) rat model of schizophrenia, Neurotox. Res. 32 (2017) 121–133, https://doi.org/10.1007/s12640-017-9718-9.
[40] M.J. Detke, M. Rickels, I. Lucki, Active behaviors in the rat forced swimming test differentially produced by serotonergic and noradrenergic antidepressants, Psychopharmacol. (Berl.) 121 (1995) 66–72, https://doi.org/10.1007/BF02245592.
[41] G. Paxinos, C. Watson, The Rat Brain in Stereotaxic Coordinates: Hard Cover Edition, Elsevier, 2006.
[42] C. Juchem, C. Cudalbu, R.A. De Graaf, R. Gruetter, A. Henning, H.P. Hetherington, V.O. Boer, B_0 shimming for in vivo magnetic resonance spectroscopy: experts' consensus recommendations, NMR Biomed. 34 (2021) e4350, https://doi.org/10.1002/nbm.4350.
[43] E. Drazanova, J. Ruda-Kucerova, L. Kratka, K. Horska, R. Demlova, Z. Starcuk, T. Kasparek, Poly(I:C) model of schizophrenia in rats induces sex-dependent functional brain changes detected by MRI that are not reversed by aripiprazole treatment, Brain Res. Bull. 137 (2018) 146–155, https://doi.org/10.1016/j.brainresbull.2017.11.008.
[44] E. Drazanova, L. Kratka, N. Vaskovicova, R. Skoupy, K. Horska, Z. Babinska, H. Kotolova, L. Vrlikova, M. Buchtova, Z. Starcuk, J. Ruda-Kucerova, Olanzapine exposure diminishes perfusion and decreases volume of sensorimotor cortex in rats, Pharmacol. Rep. 71 (2019) 839–847, https://doi.org/10.1016/j.pharep.2019.04.020.
[45] J. Vitouš, R. Jiřík, T. Stračina, M. Hendrych, J. Nádeníček, O. Macíček, Y. Tian, L. Krátká, E. Dražanová, M. Nováková, P. Babula, R. Panovský, E. DiBella, Z. Starčuk, T1 mapping of myocardium in rats using self-gated golden-angle acquisition, Magn. Reson. Med. 91 (2024) 368–380, https://doi.org/10.1002/mrm.29846.
[46] D. Stefan, F.D. Cesare, A. Andrasescu, E. Popa, A. Lazariev, E. Vescovo, O. Strbak, S. Williams, Z. Starcuk, M. Cabanas, D. Van Ormondt, D. Graveron-Demilly, Quantitation of magnetic resonance spectroscopy signals: the jMRUI software package, Meas. Sci. Technol. 20 (2009) 104035, https://doi.org/10.1088/0957-0233/20/10/104035.
[47] Z. Starčuk, J. Starčuková, Quantum-mechanical simulations for in vivo MR spectroscopy: Principles and possibilities demonstrated with the program NMRScopeB, Anal. Biochem. 529 (2017) 79–97, https://doi.org/10.1016/j.ab.2016.10.007.
[48] H. Ratiney, Y. Coenradie, S. Cavassila, D. Ormondt, D.J. Graveron-Demilly, Time-Domain Quantitation with a Metabolite Basis Set, (2003).
[49] J. Starčuková, D. Stefan, D. Graveron-Demilly, Quantification of short echo time MRS signals with improved version of quantitation based on quantum ESTimation algorithm, NMR Biomed. 36 (2023) e5008, https://doi.org/10.1002/nbm.5008.
[50] V. Belle, E. Kahler, C. Waller, E. Rommel, S. Voll, K. Hiller, W.R. Bauer, A. Haase, In Vivo quantitative mapping of cardiac perfusion in rats using a noninvasive MR spin-labeling method, J. Magn. Reson. Imaging 8 (1998) 1240–1245, https://doi.org/10.1002/jmri.1880080610.
[51] T. Arunrut, H. Alejandre, M. Chen, J. Cha, A. Russo-Neustadt, Differential behavioral and neurochemical effects of exercise, reboxetine and citalopram with the forced swim test, Life Sci. 84 (2009) 584–589, https://doi.org/10.1016/j.lfs.2009.02.005.
[52] J.F. Cryan, R.J. Valentino, I. Lucki, Assessing substrates underlying the behavioral effects of antidepressants using the modified rat forced swimming test, Neurosci. Biobehav. Rev. 29 (2005) 547–569, https://doi.org/10.1016/j.neubiorev.2005.03.008.
[53] R.A. Graaf, In Vivo NMR Spectroscopy: Principles and Techniques, 1st ed, Wiley, 2019, https://doi.org/10.1002/9781119382461.
[54] S.-T. Hong, C.-B. Choi, C. Park, H.-Y. Moon, K.S. Hong, C. Cheong, J.-H. Chae, B.-Y. Choe, Specific hippocampal choline decrease in an animal model of depression, Br. J. Radiol. 82 (2009) 549–553, https://doi.org/10.1259/bjr/25165760.
[55] D. Schulz, D. Smith, M. Yu, H. Lee, F.A. Henn, Selective breeding for helplessness in rats alters the metabolic profile of the hippocampus and frontal cortex: a 1H-MRS study at 9.4 T, Int. J. Neuropsychopharmacol. 16 (2013) 199–212, https://doi.org/10.1017/S1461145711001994.
[56] C.-H. Yoo, S.-I. Lim, K.-H. Song, D.-C. Woo, B.-Y. Choe, Investigating the metabolic alterations in a depressive-like rat model of chronic forced swim stress: an in vivo proton magnetic resonance spectroscopy study at 7T, Neurochem. Int. 116 (2018) 22–29, https://doi.org/10.1016/j.neuint.2018.03.005.
[57] H. Zhang, G. Yan, H. Xu, Z. Fang, J. Zhang, J. Zhang, R. Wu, J. Kong, Q. Huang, The recovery trajectory of adolescent social defeat stress-induced behavioral, 1H-MRS metabolites and myelin changes in Balb/c mice, Sci. Rep. 6 (2016) 27906, https://doi.org/10.1038/srep27906.
[58] J. Ritter, R.J. Flower, G. Henderson, Y.K. Loke, D.J. MacEwan, E.S.J. Robinson, J. Fullerton. Rang and Dale's pharmacology, Tenth edition, Elsevier, London, 2024.
[59] L.F. Saccaro, M. Tassone, F. Tozzi, G. Rutigliano, Proton magnetic resonance spectroscopy of N-acetyl aspartate in first depressive episode and chronic major depressive disorder: a systematic review and meta-analysis, J. Affect. Disord. 355 (2024) 265–282, https://doi.org/10.1016/j.jad.2024.03.150.
[60] S. Ramírez-Guerrero, S. Guardo-Maya, G.J. Medina-Rincón, E.E. Orrego-González, R. Cabezas-Pérez, R.E. González-Reyes, Taurine and astrocytes: a homeostatic and neuroprotective relationship, Front. Mol. Neurosci. 15 (2022) 937789, https://doi.org/10.3389/fnmol.2022.937789.
[61] S. Biedermann, W. Weber-Fahr, L. Zheng, C. Hoyer, B. Vollmayr, P. Gass, G. Ende, A. Sartorius, Increase of hippocampal glutamate after electroconvulsive treatment: a quantitative proton MR spectroscopy study at 9.4 T in an animal model of depression, World J. Biol. Psychiatry 13 (2012) 447–457, https://doi.org/10.3109/15622975.2011.580778.
[62] G. Xi, J. Hui, Z. Zhang, S. Liu, X. Zhang, G. Teng, K.C. Chan, E.X. Wu, B. Nie, B. Shan, L. Li, G.P. Reynolds, Learning and memory alterations are associated with hippocampal N-acetylaspartate in a rat model of depression as measured by 1H-MRS, PLoS ONE 6 (2011) e28686, https://doi.org/10.1371/journal.pone.0028686.
[63] D. Rial, C. Lemos, H. Pinheiro, J.M. Duarte, F.Q. Gonçalves, J.I. Real, R.D. Prediger, N. Gonçalves, C.A. Gomes, P.M. Canas, P. Agostinho, R.A. Cunha, Depression as a glial-based synaptic dysfunction, Front. Cell. Neurosci. 9 (2016), https://doi.org/10.3389/fncel.2015.00521.
[64] S. Gormley, J. Rouine, A. McIntosh, C. Kerskens, A. Harkin, Glial fibrillary acidic protein (GFAP) immunoreactivity correlates with cortical perfusion parameters determined by bolus tracking arterial spin labelling (bt-ASL) magnetic resonance (MR) imaging in the Wistar Kyoto rat, Physiol. Behav. 160 (2016) 66–79, https://doi.org/10.1016/j.physbeh.2016.04.007.
[65] N. Gass, D. Cleppien, L. Zheng, A.J. Schwarz, A. Meyer-Lindenberg, B. Vollmayr, W. Weber-Fahr, A. Sartorius, Functionally altered neurocircuits in a rat model of treatment-resistant depression show prominent role of the habenula, Eur. Neuropsychopharmacol. 24 (2014) 381–390, https://doi.org/10.1016/j.euroneuro.2013.12.004.
[66] A.L. McIntosh, S. Gormley, L. Tozzi, T. Frodl, A. Harkin, Recent advances in translational magnetic resonance imaging in animal models of stress and depression, Front. Cell. Neurosci. 11 (2017) 150, https://doi.org/10.3389/fncel.2017.00150.
[67] S. Passero, M. Nardini, N. Battistini, Regional cerebral blood flow changes following chronic administration of antidepressant drugs, Prog. Neuropsychopharmacol. Biol. Psychiatry 19 (1995) 627–636, https://doi.org/10.1016/0278-5846(95)00107-7.
[68] Y. Kaichi, G. Okada, M. Takamura, S. Toki, Y. Akiyama, T. Higaki, Y. Matsubara, Y. Okamoto, S. Yamawaki, K. Awai, Changes in the regional cerebral blood flow detected by arterial spin labeling after 6-week escitalopram treatment for major depressive disorder, J. Affect. Disord. 194 (2016) 135–143, https://doi.org/10.1016/j.jad.2015.12.062.
[69] A.Y. Joe, T. Tielmann, J. Bucerius, M.J. Reinhardt, H. Palmedo, W. Maier, H.-J. Biersack, A. Zobel, Response-dependent differences in regional cerebral blood flow changes with citalopram in treatment of major depression, J. Nucl. Med. Off. Publ. Soc. Nucl. Med. 47 (2006) 1319–1325.
[70] R. Viviani, B. Abler, A. Seeringer, J.C. Stingl, Effect of paroxetine and bupropion on human resting brain perfusion: an arterial spin labeling study, NeuroImage 61 (2012) 773–779, https://doi.org/10.1016/j.neuroimage.2012.03.014.
[71] R.L. Carhart-Harris, K. Murphy, R. Leech, D. Erritzoe, M.B. Wall, B. Ferguson, L.T. J. Williams, L. Roseman, S. Brugger, I. De Meer, M. Tanner, R. Tyacke, K. Wolff, A. Sethi, M.A.P. Bloomfield, T.M. Williams, M. Bolstridge, L. Stewart, C. Morgan, R. D. Newbould, A. Feilding, H.V. Curran, D.J. Nutt, The Effects of acutely administered 3,4-methylenedioxymethamphetamine on spontaneous brain function in healthy volunteers measured with arterial spin labeling and blood oxygen level–dependent resting state functional connectivity, Biol. Psychiatry 78 (2015) 554–562, https://doi.org/10.1016/j.biopsych.2013.12.015.
[72] D.E. McBean, I.M. Ritchie, H.J. Olverman, P.A.T. Kelly, Effects of the specific serotonin reuptake inhibitor, citalopram, upon local cerebral blood flow and glucose utilisation in the rat, Brain Res 847 (1999) 80–84, https://doi.org/10.1016/S0006-8993(99)02033-8.
[73] A. Klomp, M.W.A. Caan, D. Denys, A.J. Nederveen, L. Reneman, Feasibility of ASL-based phMRI with a single dose of oral citalopram for repeated assessment of serotonin function, NeuroImage 63 (2012) 1695–1700, https://doi.org/10.1016/j.neuroimage.2012.07.038.
[74] Y. Chen, H.I. Wan, J.P. O'Reardon, D.J.J. Wang, Z. Wang, M. Korczykowski, J. A. Detre, Quantification of cerebral blood flow as biomarker of drug effect: arterial spin labeling phmri after a single dose of oral citalopram, Clin. Pharmacol. Ther. 89 (2011) 251–258, https://doi.org/10.1038/clpt.2010.296.
[75] J. Geday, F. Hermansen, R. Rosenberg, D.F. Smith, Serotonin modulation of cerebral blood flow measured with positron emission tomography (PET) in humans, Synapse 55 (2005) 224–229, https://doi.org/10.1002/syn.20112.
[76] M.M. Solleveld, A. Schrantee, J.R. Homberg, P.J. Lucassen, L. Reneman, The influence of age-of-onset of antidepressant use on the acute CBF response to a citalopram challenge; a pharmacological MRI study, Psychiatry Res. Neuroimaging 303 (2020) 111126, https://doi.org/10.1016/j.pscychresns.2020.111126.